Radiative and nonradiative recombination in polymerlike *a*-C:H films

T. Heitz, C. Godet, J. E. Bourée, and B. Drévillon
Laboratoire de Physique des Interfaces et des Couches Minces (UMR 7647 CNRS) Ecole Polytechnique, 91128 Palaiseau Cedex, France

J. P. Conde
IST, Department of Materials Engineering, Avenida Rovisco Pais, 1096 Lisboa, Portugal
(Received 28 December 1998; revised manuscript received 12 April 1999)

Localized electronic states corresponding to π electrons in hydrogenated amorphous carbon have been investigated using photoluminescence (PL) and optical-absorption spectroscopies. Carbon films contain π-bonded ''grains'' with different configurations which spatially confine photogenerated electron-hole pairs. A model of PL in *a*-C:H, including excitonlike radiative recombination and electron tunneling to nonradiative acceptor centers at constant energy, is proposed to explain the following results. The broad PL emission spectra are composed of three bands (at 2.20–2.40 eV, 2.65 eV, and 2.95 eV, independent of the excitation energy) arising from different structural units containing C═C double bonds. Resonance features have been evidenced in the PL excitation spectra and attributed to excitation of confined electron-hole pairs similar to confined exciton optical transitions. Excitonic behavior is consistent with the redshift of peak (b) excitation resonance observed as a function of increasing gap (decreasing ε). Relative values of the radiative rates deduced from PL efficiency indicate that the exciton radius has the same order of magnitude for all three emissive centers. Nonradiative recombination cannot be explained by multiphonon emission processes. The dependence of PL efficiency on the density of acceptor sites (deduced from $\pi-\pi^*$ optical transitions) can rather be described by electron tunneling from a confined exciton toward nonradiative localized π^* states arising from distorted π-bonded sites. This mechanism accounts for the anticorrelation of the PL efficiency with the optical gap, the decrease of the decay time as a function of emission energy, and the relative enhancement of the blue emission (2.95-eV peak) as a function of decreasing optical gap. In contrast, the band-tail model proposed earlier leads to unrealistically low values of the electron Bohr radius. [S0163-1829(99)12031-9]

I. INTRODUCTION

The microscopic structure of hydrogenated amorphous carbon (*a*-C:H) covers a very wide range, intermediate between polymers and covalent amorphous solids. The electronic properties of *a*-C:H are expected to be controlled by π-bonding molecular orbitals, as generally occurs in π-bonded systems, with, however, a strong influence of disorder and local stress related to the degree of cross-linking of the matrix. As in polymers,[1] the description of absorption and photoluminescence properties in terms of either single-carrier band-tail states or excitons remains a matter of debate.

Amorphous carbon thin films contain mainly sp^2- and sp^3-hybridized atoms, in line with the assumption that sp^1 configurations cannot coexist with sp^3 bonding under thermodynamic equilibrium.[2] The bonding structure of *a*-C:H is complex for several reasons: (i) sp^2 sites tend to gather into pairs or larger conjugated clusters[3] (forming olefinic chains or aromatic rings), hence relieving some topological constraints[4]; (ii) films prepared from hydrocarbon dissociation may incorporate high bonded H densities (up to $\approx$60 at. %) which act as inhibitor of aromatic clustering and make the C skeleton weakly cross-linked (polymerlike carbon); (iii) π-molecular orbitals at sp^2-hybridized sites are responsible for low-binding-energy states which control the optical gap and other electronic properties; (iv) strong site-to-site potential fluctuations result from the large difference between π and σ bond energies, which in turn lead to low carrier mobilities and strong luminescence efficiency at room temperature. Understanding the degree of clustering of C═C double bonds and H bonding to the C skeleton[5] is thus a key issue to control the electronic properties of *a*-C:H and improve the properties of C-based optoelectronic devices, such as light-emitting diodes[6] and thin-film cold cathodes for field emission displays.[7]

Extended electronic states lie in the σ and σ^* bands, well beyond the localized π and π^* states which form the band-edge distributions[8] and control optical and photoluminescence (PL) properties.[3,9–12] It has been argued that hydrogen incorporation contributes to some localization of π electrons and formation of potential barriers for carriers confined in polyaromatic clusters.[10,13] Photoluminescence is a powerful site-selective spectroscopy to investigate localized electronic states within the band gap of amorphous semiconductors.[14,15] Although it is widely recognized that the large density of localized states related to π bonds may trap photogenerated electron-hole pairs and be responsible for the strong radiative recombination, different hypotheses for luminescent centers and quenching mechanisms in *a*-C:H have been discussed in recent reviews.[3,13,16]

A first approach[3] to describe PL in *a*-C:H aims at extending a model proposed for PL properties of *a*-Si:H.[14,15] The absorption of a photon creates an electron-hole pair whose wave functions initially overlap. In the limit of weak Coulomb interaction, the photogenerated electron and hole diffuse apart, while they thermalize independently in their respective band-tail states. The thermalized electron and hole

recombine radiatively by tunneling, provided that they lie beyond a critical tunneling distance from a threefold-coordinated Si atom acting as a nonradiative defect. However, the microscopic identification of nonradiative centers in *a*-C:H is not yet clear, and the correlation between electron-spin-resonance (ESR)-active defects and PL efficiency is not established.[17,18]

A second approach is based on the peculiar PL properties of *a*-C:H as compared to *a*-Si:H, namely, a sizable anti-Stokes photoluminescence,[9,11] a lack of temperature quenching of PL efficiency,[9] and a strong photoluminescence polarization memory[11,19] which indicate a strong electron-hole Coulomb interaction (favored by the low ε value) and may suggest an excitonlike behavior. In the latter model of polymerlike carbon, electronic properties arise from a *distribution* of independent π-bonded ''grains''[9] which provide a strong spatial confinement of excitonlike entities. In this description, a quantitative estimation of the confinement is lacking and the nonradiative channel remains unexplained.

The aim of this paper is to investigate UV-visible optical and photoluminescence properties (using steady-state emission and excitation spectroscopies) of plasma-deposited polymerlike carbon films. Our data are used to build the basis of a model for radiative and nonradiative recombination channels in polymerlike *a*-C:H, in relation with the film nanostructure.

II. EXPERIMENT

Hydrogenated amorphous carbon (*a*-C:H) films have been grown on the rf electrode of a radiofrequency-assisted microwave reactor[20,21] using *n*-butane as a carbon precursor injected in the microwave (MW) post-discharge. Carbon films were grown on single crystal silicon (*c*-Si) to avoid PL from the substrate. The energy of positive ions impinging on the growing surface increases from 20 to 140 eV (due to the negative self-bias voltage) for increasing nominal rf power (20–100 W). The role of H-atom flux interacting with the growing film has been shown by comparing different mixtures (Ar-H_2 or Ar-He) in the MW plasma, providing high and low H-atom flux, respectively. The growth mechanisms have been described previously in terms of ion-induced activation of surface sites available for chemisorption of C_xH_y or H radicals.[21]

The UV-visible ellipsometry technique has been used to monitor changes in optical transitions between bonding π states and antibonding π^* states arising from structural elements containing C=C double bonds. π and σ orbitals being considered as completely decoupled,[22] measurements in the range 1.5–4.5 eV were parametrized using an analytic dielectric function based on the Forouhi-Bloomer approximation[23] which consists of computing electronic transitions between parabolic density-of-states distributions separated by a forbidden gap (defined as E_g). As sketched in Fig. 7, $(E_{\pi^*}-E_\pi)$ represents the average gap between the distributions of electronic states corresponding to bonding (π) and antibonding (π^*) orbitals and the optical gap E_{04} is obtained at an absorption coefficient $\alpha(E_{04})=10^4\,\mathrm{cm}^{-1}$.

Although the approximation of parabolic bands fails to describe the exponential tails in the electronic density of states in the region of the forbidden gap, the accuracy of the parametrization in the high absorption range has been shown in a previous paper (Ref. 21). In this range, parabolic and Gaussian approximations provide equally good fitting, while the latter leads to significantly higher values of $(E_{\pi^*}-E_\pi)$. However, the values of $(E_{\pi^*}-E_\pi)$ obtained from the Forouhi-Bloomer model are within or close to the range of ellipsometry measurements, meaning that extrapolation problems can be avoided.

TABLE I. Plasma parameters for *a*-C:H films grown using the dual-plasma technique with Ar-H_2 (250–40 sccm) gas mixtures at 300 mTorr.

Film	E_{04} (eV)	d (nm)	Microwave power (W)	rf power (W)	Butane flow rate (sccm)	T_S (°C)
A	3.45	250	400	60	40	70
B	2.85	300	400	80	40	70
C	2.60	270	400	100	40	70
D	4.10	130	400	30	40	70
E	3.30	64	400	60	40	250
F	3.80	230	300	50	40	70
G	3.70	250	200	50	40	70
H	3.05	200	400	70	40	70

Photoluminescence measurements were performed at room temperature with a SPEX Fluorolog system. Unpolarized UV light from a Xe arc lamp is focused onto the sample through a monochromator (4.5-nm excitation bandwidth) at an incidence angle ≈50°–70°. The resulting photoluminescence is collected by a monochromator (2.25-nm emission bandwidth) coupled with a photomultiplier tube. The system optical response has been calibrated using a solution of rhodamine and the normalized spectral density $W(E_{\mathrm{em}}) = W(\lambda_{\mathrm{em}})/E_{\mathrm{em}^2}$ has been obtained after taking into account the film absorbance at excitation energy E_{exc}, the film reabsorption at emission energy E_{em}, and the change of the emitted flux brightness at the *a*-C:H/air interface.[24] No correction has been made for the weak interferences inside 60–300-nm-thick films.

III. RESULTS

A. Stoichiometry and density

Polymerlike carbon films with low density ($\rho \leqslant 1.8\,\mathrm{g\,cm}^{-3}$) and high H content (35–50 at. %) have been grown. The densification induced by ion bombardment leads to an increase of the local coordination number n_{C-C} and local stress.[25] Large variations of optical parameter values have been observed as a function of the deposition conditions, the wider band gaps ($E_g \approx 3$ eV or $E_{04} \approx 4$ eV) being obtained using a high H-atom flux (Table I). A monotonic decrease of E_g is observed for increasing rf power, i.e. increasing mean ion energy, and the same trend is found on both E_{04} and $(E_{\pi^*}-E_\pi)$ variations.[21]

Basically the optical gap values are related to microstructural changes which mainly result from a competition between ion bombardment and H-atom flux impinging on *a*-C:H films. Combining optical measurements and Rutherford backscattering, the *joint density of π states* is found to

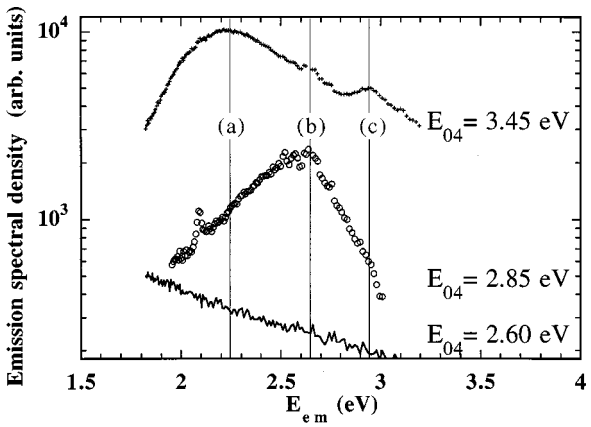

FIG. 1. Spectral density $W(E_{\mathrm{em}})$ of PL emission for films *A* (3.45 eV), *B* (2.85 eV), and *C* (2.60 eV) (Table I), showing the existence of three peaks, for excitation at $E_{\mathrm{exc}}=3.54$ eV.

be directly related to the mass density of polymerlike carbon films in the range 1.1–1.8 $\mathrm{g\,cm^{-3}}$, independent of the particular plasma parameters.[21]

B. Photoluminescence emission spectroscopy

In a previous PL emission study using Ar^+ laser excitation at 2.54 eV, we found[25,26] a single broad Gaussian peak centered at 2.0–2.3 eV, in agreement with other reports.[11,27] In contrast, PL emission spectra excited with UV photons appear as composed of three bands with specific energy positions [hereafter labeled as (a) 2.20–2.40 eV, (b) 2.65 eV, and (c) 2.95 eV]. Figure 1 shows the emission spectral density $W(E_{\mathrm{em}})$ normalized to the number of absorbed photons for films *A*, *B*, and *C*, grown with increasing ion energy. The intermediate condition shows unambiguously the existence of peak (b). In a previous report, the peak (b) intensity decay time was found to be about 50 ps, intermediate between peaks (a) and (c) typical values, respectively 200 and 5 ps.[28] It has also been checked that the existence of three bands is not plasma reactor dependent and that their relative intensities depend on plasma treatment.[28] For increasing rf power in the dual plasma deposition of *a*-C:H films, the optical gap E_{04} decreases from 4.0 to 1.5 eV, and peak (a) is found to shift slightly from 2.4 to 2.2 eV.

Figure 2 shows the emission spectral density $W(E_{\mathrm{em}})$ for films *D* and *E*, which were chosen for their similar high PL efficiencies and different absorption edges. As a general result, the normalized spectra obtained at different E_{exc} values (3.54 or 4.13 eV) give evidence of a lower PL efficiency for the latter excitation energy. However, the positions and widths of the three emission bands are independent on the excitation energy. Although an accurate decomposition into three Gaussian peaks could not be obtained, we observe a decrease of the full width at half maximum, from band (a) to band (c): $\mathcal{F}(\mathrm{a})\approx 0.6$ eV and $\mathcal{F}(\mathrm{c})\approx 0.3$ eV.

The amplitude and integrated intensity of $W(E_{\mathrm{em}})$ for each peak being dependent on the assumption of Gaussian peaks their respective evolution can only be considered as global tendencies. Figure 3 reports the intensity ratio between peaks (b) and (c) for increasing optical gap. As the intensities of peaks (a), (b), and (c) monotonously decrease as a function of decreasing optical gap, some spectral modifications occur, namely, an enhancement of the blue part of the broad PL emission. It will be underlined below that this behavior is opposite to the effects expected from carrier thermalization into a broadening band-tail distribution, as found in *a*-Si:H.[14,15]

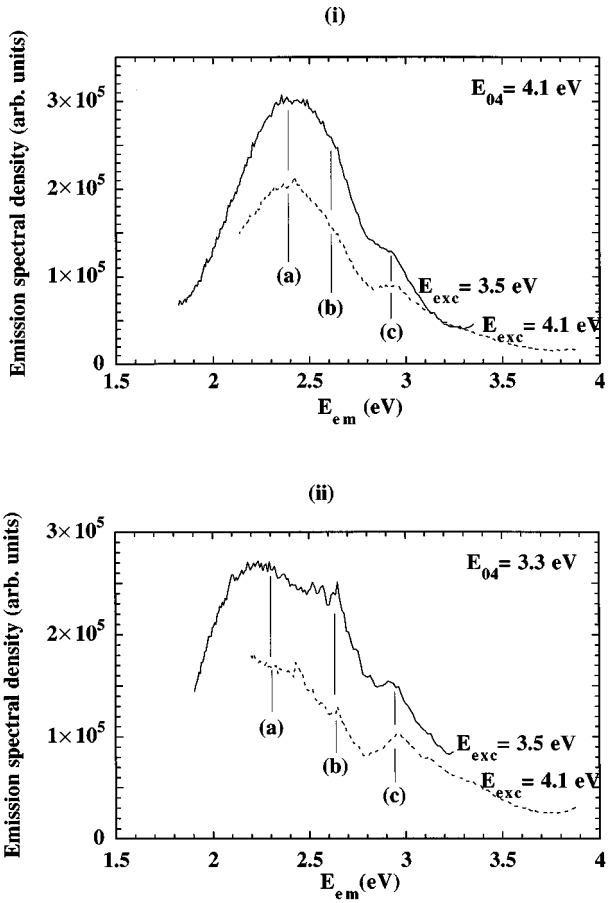

FIG. 2. Normalized spectral density $W(E_{\mathrm{em}})$ for films *D* (4.10 eV) and *E* (3.30 eV) (Table I), for excitation at $E_{\mathrm{exc}}=3.54$ eV (continuous line) and 4.13 eV (dotted line).

C. Photoluminescence excitation spectroscopy

The excitation spectral density was not normalized due to the low accuracy of absorption values near the absorption

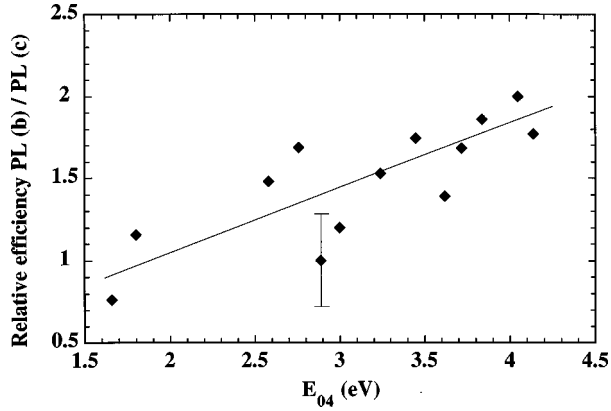

FIG. 3. Relative efficiency of peaks (b) and (c) as a function of the optical gap E_{04} ($E_{\mathrm{exc}}=3.54$ eV).

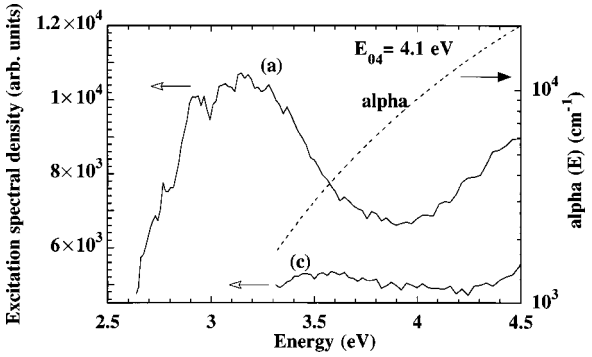

FIG. 4. Absorption coefficient (alpha) and PL excitation spectra for film *D* (4.10 eV). The spectral density $W(E_{\rm exc})$ corresponds to PL emission at 2.40 eV [band (a)] and 2.95 eV [band (c)].

edge. However, it is clear that the PL excitation spectra [at selected emission energies belonging to peaks (a), (b), and (c)] are *not correlated* with the absorption coefficient spectra, as could be expected.

The PL intensity of peak (c) is generally independent on excitation energy $E_{\rm exc}$ above 3.3 eV (Fig. 4). A different behavior is found at lower emission energies: for most of the investigated films, the excitation spectra can be described by a sharp threshold [as shown for peak (a) in Fig. 4] followed by either a decrease or by oscillations around a mean value of the PL efficiency. As far as ''resonance'' effects in excitation spectra are concerned, the more prominent features have been found for peak (b) (2.65 eV), as illustrated in Fig. 5. These maxima occur in the range 3.2–3.6 eV, and a significant redshift of resonance energy occurs for increasing values of the optical gap.

D. PL efficiency

The dependence of the relative PL efficiency on the ion energy during growth being similar for the three emission bands,[28] we focus our attention on the more intense peak (a) which has been widely characterized in the literature. Considering the photoluminescence spectral density $W(E_{\rm em})$ at peak (a) maximum, W(a) values span more than three orders of magnitude (Fig. 6) for our dual-plasma *a*-C:H films. We find that the PL efficiency is strongly correlated to the UV-visible optical properties (at 3.5 eV) in line with previous

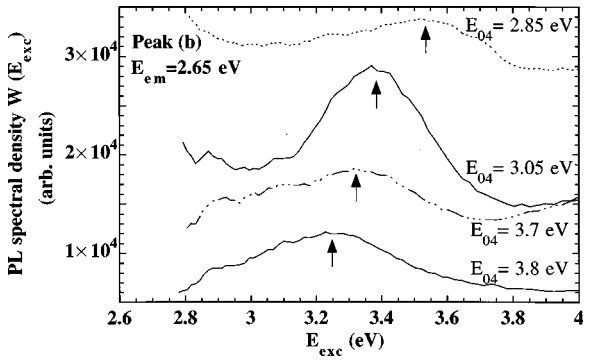

FIG. 5. Spectral density $W(E_{\rm exc})$ corresponding to peak (b) emission at 2.65 eV, showing resonance features, for *a*-C:H with decreasing values of the optical gap (films *F*, *G*, *H*, and *B* from Table I).

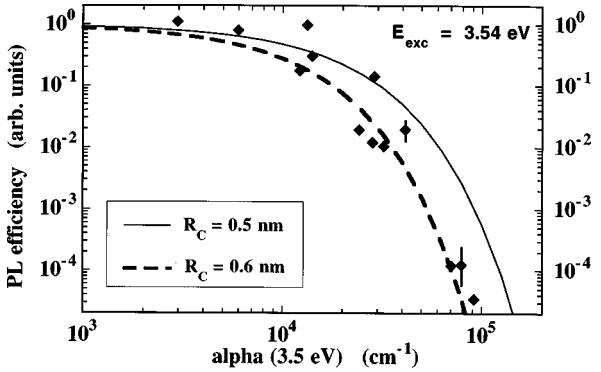

FIG. 6. Dependence of the photoluminescence efficiency of band (a) (obtained with $E_{\rm exc}=3.54$ eV) on the absorption coefficient α (3.5 eV). The model based on nonradiative tunneling to defect states is taken from Ref. 14.

observations.[10,12,25,29] The arbitrary choice of a photon energy of 3.5 eV, located between $E_{\rm em}$ and $E_{\rm exc}$, will be discussed below.

For optical excitation between π and π^* states, the estimation of the transition matrix element is not straightforward in a disordered material which may contain a variety of π-conjugated configurations. Our previous estimate[29] of an optical cross section based on column-IV amorphous semiconductors ($\sigma_{a\text{-Si:H}}=3\times10^{-17}\,{\rm cm}^2$) should be revised to lower values. In fact, the nature of the states involved in the transitions responsible for UV-visible absorption are fundamentally different in *a*-C:H and *a*-Si:H, both for orbital symmetry and for spatial localization reasons. Although the optical matrix element may also depend on the detailed microstructure of the carbon matrix, in the following we will use an estimate $\sigma_{a\text{-C}}=7\pm3\times10^{-18}\,{\rm cm}^2$, obtained from the ratio of the absorption coefficient (using $k=1.5$ at 3.2 eV)[30] to the atom density ($7.5\times10^{22}\,{\rm cm}^{-3}$) in evaporated glassy carbon which is close to one π electron per C atom.

Using this hypothesis, the absorption values reported in Fig. 6 thus correspond to density of states values $N_{\rm opt}$ between 4×10^{20} and $1.3\times10^{22}\,{\rm cm}^{-3}$. It is stressed that the value of $(E_{\pi^*}-E_{\pi})$ decreases between 5.5 and 2.5 eV for increasing film density,[21] which is attributed to lattice distortions.[31] As a consequence, α(3.5 eV) or $N_{\rm opt}$ is basically a signature of distorted π-bonded sites, i.e., underestimating the total number of π-bonded sites. For comparison on the same films, the density of hydrogenated olefinic sp^2 carbon atoms has been evaluated from the bending vibrational mode,[5] and found to increase from 5×10^{20} to $3\times10^{21}\,{\rm cm}^{-3}$.

IV. RECOMBINATION MODEL

The radiative recombination of a photogenerated electron-hole pair follows a fast thermalization process ($\approx10^{-13}$–10^{-12} s) in which both carriers exchange some excess energy with the medium (Fig. 7) while feeling the influence of disorder-induced potential fluctuations of the solid and the attractive Coulomb interaction of the geminate carrier. The hole coupling to the lattice is usually considered to be stronger than electron coupling.[32] Radiative and nonradiative mechanisms occur in the 1 ps–1 ns range, i.e., after

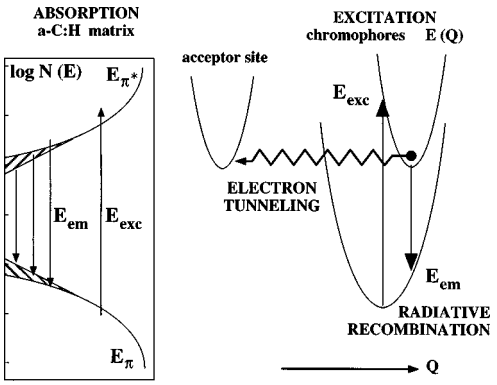

FIG. 7. Absorption of a-C:H matrix (band model) and PL excitation of chromophores (local configuration model). After excitation at energy $E_{\rm exc}$ and fast thermalization of the photogenerated pair, the nonradiative dissociation (electron tunneling toward vacant distorted π^* states in the host matrix) competes with light emission at energy $E_{\rm em}$. Nonradiative multiphonon emission processes can be neglected.

thermalization is completed. In order to describe experimental PL data reported in Sec. III, some possible radiative and nonradiative mechanisms are discussed below in the framework of two models, the *one-electron band-tail* model and the *confined excitonlike electron-hole* pair model.

A. Nonradiative recombination

Nonradiative recombination may occur through several mechanisms including multiphonon emission or carrier excitation to a conduction path where the trapping at a nonradiative center is efficient. In wide-band-gap a-C:H, the multiphonon emission is ruled out on the basis of calculations made below in Sec. IV C. Since neither thermal quenching nor electric-field quenching of the PL efficiency could be observed in a-C:H films,[9] one can infer a strong binding of the electron-hole pair, which is consistent with the very low carrier mobility experimentally measured in polymerlike a-C:H.[33]

Hence two hypotheses may be formulated for PL quenching, corresponding respectively to typical situations found in semiconductors and organic molecules: (i) in the one-electron model, the electron may escape from the geminate hole interaction range by a tunneling mechanism at constant energy, toward either a nonradiative site or a radiative center holding a nongeminate hole. (ii) In the exciton model, a Förster energy transfer[24] via dipole-dipole interactions requires that the spectral density of initial sites overlap with the absorption spectrum of final sites.

The respective nonradiative mechanisms may be specific to each kind of material. However, in both cases it appears that final electronic states available for tunneling or energy transfer are those located in a range between excitation energy $E_{\rm exc}$ and emission energy $E_{\rm em}$. In this framework, a strong correlation between PL efficiency and the optical properties in the range $E_{\rm em}<E<E_{\rm exc}$ is expected, as observed for polymerlike a-C:H in Fig. 6.

In addition, it is expected that both mechanisms may lead to an efficient decrease of the anisotropy of PL excited with linearly polarized light. In principle, the electron tunneling and dipole-dipole mechanisms can be distinguished due to their different dependence on the initial site to final site distance, respectively short-range exponential and medium-range power-law (d^{-6}) functions. Although it is not obvious to determine the distribution of relative distances between radiative and nonradiative centers, optical data may give some relevant insight on the states located near midgap.

Let us consider the nonradiative path as a transfer from molecularlike light-emitting species (chromophore described in a local configuration coordinate diagram) towards electronic states of the host matrix (described in a semiconductor-like band diagram), as sketched in Fig. 7. We make the strong assumption that a majority of distorted π-bonded sites in the host matrix (with a density $N_{\rm opt}$ measured by optical absorption) act as *nonradiative* centers. An estimate of the nonradiative acceptor density can thus be deduced from the absorption coefficient at an energy of 3.5 eV, selected arbitrarily. Figure 6 shows a unique correlation over several orders of magnitude between the PL efficiency and the density of optically active states $N_{\rm opt}$ (in the range 4×10^{20}–$1.3\times10^{22}\,{\rm cm}^{-3}$ as calculated above). However, it is stressed that acceptor states do not coincide with ESR-active sites since the density of spins[34] represents less than 1% of the $N_{\rm opt}$ values estimated in Sec. III D.

B. Electron tunneling (bandtail model)

Following the model developed to describe the PL properties of a-Si:H,[14,15] the tunneling rate to a nonradiative defect at a distance R is given by

$$(1/\tau_{\rm tunnel})=\nu_0\exp(-2R/R_0). \tag{1}$$

If one assumes that the density of optically measured states ($N_{\rm opt}$) can be identified with the density of nonradiative defects, and that defects and photogenerated carriers are randomly distributed, the photoluminescence efficiency is the probability

$$(Y/Y_0)=\exp[-(4\pi/3)R_C{}^3N_{\rm opt}] \tag{2}$$

of not finding a defect within R_C of a given point. The critical radius R_C is related to the Bohr radius R_0 and the radiative lifetime ($\tau_{\rm rad}$): $2R_C/R_0=Ln(\nu_0\tau_{\rm rad})$.

In the band-tail model, the fitted value of $R_C=6\pm1$ Å (Fig. 6), the phonon frequency $\nu_0=10^{13}\,{\rm s}^{-1}$ in a-C:H, and the typical value of $(\tau_{\rm rad})\approx1$ ns assumed for the radiative lifetime[34] allow the determination of a Bohr radius $R_0\approx1.3\pm0.4$ Å (i.e., one interatomic distance). Although the tunneling concept seems to be consistent with the experiment, the latter value of the Bohr radius R_0 appears to be extremely small. Data are thus compared to the exciton model developed in the next section.

C. Electron tunneling (exciton model)

Previous data on the polarization memory of photoluminescence[11,19] and evidence of resonance features in PL excitation spectra (Figs. 4 and 5) are strong indications that the recombining species behave similarly to confined excitons. According to the Kivelson-Gelatt model for PL in amorphous materials,[32] one may suppose that the self-trapping in a π-bonded ''grain'' is governed by the positive

hole, and that the electron will also be trapped due to a strong Coulomb interaction. The PL spectral characteristics are thus expected to depend on the depth of the hole trapping at local lattice deformations, while the electron would be responsible for the exciton dissociation rate.

The hydrogenoid model is applied to calculate the exciton radius $a_B^* = (4\pi\varepsilon_0\varepsilon\hbar^2)/\mu^* e^2$, where μ^* is the analog of a reduced mass ($\mu^* \approx m_e^* \approx 0.25 m_e$), and ε the dielectric constant. If the electron-hole distance or the size of the confining well are too small, this equation would require some corrections. The exciton radius increases as a function of the dielectric constant, related to the *a*-C:H film density.[5] Using $\varepsilon = 3$ as a typical value in polymerlike *a*-C:H, an estimate of $a_B^* \approx 6$ Å is obtained along with $E_B = 0.40$ eV, where the corresponding binding energy is $E_B = e^2/8\pi\varepsilon_0\varepsilon a_B^*$ which stabilizes the exciton with respect to an electron sitting at the bottom of a ''grain'' well. This equation is qualitatively consistent with the red shift of peak (b) excitation resonance as a function of increasing gap (decreasing ε).

Excitonlike recombination

Since an exact expression of the confined electron and hole wave functions would be very complex, we only aim at deriving basic tendencies for the radiative and nonradiative recombination rates as a function of exciton localization. Although olefinic chains or aromatic rings are strongly anisotropic, we will assume that a spherical approximation holds with a radial decay given by an effective electron Bohr radius. The radius of the hole state (a_H) and the exciton radius (a_{B1}^*) determine the radiative recombination rate. The radiative transition is described as a dipolar electric transition of an electron from an initial state to an unoccupied final state separated by an energy $E_{\rm em}$. The radiative transition rate[25]

$$P_R = Cte\ \varepsilon^{1/2} E_{\rm em} 3 (a_{B1}^* a_H^*)^5 / (a_{B1}^* + a_H^*)^8 \qquad (3)$$

is approximated by $P_R \approx \varepsilon^{1/2} E_{\rm em} 3 a^5 / (a_{B1}^*)^3$ if the hole radius is close to one interatomic distance (a) with (a) $\ll (a_{B1}^*)$. The radiative rate being a power-law function of the exciton radius, its dependence on the dielectric constant cannot explain the observed change of PL efficiency over several orders of magnitude.

Hence, the nonradiative lifetimes govern the experimental PL decay times. Combining PL efficiency data and decay times values, our results indicate that the radiative lifetimes, and hence the values of the Bohr radius, have the same order of magnitude for exciton-like species corresponding to emission bands (a), (b), and (c).

Exciton dissociation

First we show that the nonradiative recombination channel via multiphonon emission can be ruled out in polymerlike carbon films. The nonradiative recombination rate of a bound exciton via multiphonon emission, which is valid when the hole is localized on a single lattice site,[32] is

$$P_{\rm NR}(s^{-1}) = 10^{13} (2a_H / a_{B1}^*)^3 \exp(-\Delta E/\hbar\omega_0), \qquad (4)$$

where $\hbar\omega_0 \approx 0.37$ eV is the phonon energy given by localized C-H vibrations, and $\Delta E \approx 2.3$ eV is the exciton energy. For $a_H \approx 1$ Å and $a_{B1}^* \approx 6$ Å, the multiphonon emission times are above 1 ns and thus *cannot* account for the shorter experimental decay times found in *a*-C:H.[28,36,37] However, Eq. (4) shows that an exchange of one or two phonons with the medium is a fast process which may be considered as one of the possible mechanisms which contribute to partial depolarization of PL.[11]

In the following, we consider the dissociation of an excitonic electron-hole pair mediated by the tunneling of the electron in site (1) to an acceptor site (2) at the same energy. Let us define as a_{B1}^* and a_{B2}^* the spatial extension of the electron wavefunction in sites (1) and (2) respectively. In the isotropic approximation of the quantum defect (spherical wave function) the initial state is described by a hydrogenoid wavefunction $\Psi_{D1}(r) = (\pi a_{B1}^* 3)^{1/2} \exp(-r/a_{B1}^*)$. The transition probability $P_{1\to 2}$ depends on the mean tunneling distance $\langle R \rangle \approx N(E_{\rm em})^{-1/3}$ to π-bonded acceptor sites at energy $E_{\rm em}$:

$$P_{1\to 2}(R) = K\varepsilon^{1/2} E_{\rm em} 3 (a_{B1}^*)^5 (a_{B2}^*)^{-3} \times \exp[-2(R - 3a_{B1}^*)/a_{B2}^*], \qquad (5)$$

which holds only if $R > (3a_{B1}^*)$. The important point is that Eq. (5) has an exponential dependence on site separation R, which indicates that exciton dissociation mechanisms may be consistent with the PL efficiency data shown in Fig. 6.

V. CONCLUDING REMARKS

It is expected that a direct relationship exists between the film density, the nanostructure, and the electronic properties,[38] and hence with the radiative recombination processes in polymerlike amorphous carbon. As the film density increases from a floppy polymerlike carbon to a denser highly cross-linked carbon, a transition has been evidenced at a film density $\rho \approx 1.3\ {\rm g\,cm^{-3}}$ from a nearly constant high PL efficiency value to a fast decreasing PL efficiency.[39]

A model including photogeneration of trapped excitonlike pairs with a typical radius (a_{B1}^*) ≈ 6 Å, exciton-like radiative transitions, and tunneling transitions at constant energy to nonradiative distorted sites has been developed and compared to the one-electron band-tail model imported from PL studies in *a*-Si:H.

The band-tail model proposed earlier leads to unrealistically low values of the electron Bohr radius. In the band-tail model, the value of the Bohr radius R_0 deduced from this study (1.4 Å) is quite small, and much smaller than an earlier reported value ($R_0 = 5.7$ Å) based on the same nonradiative tunneling hypothesis.[10] However, a number of experimental data are difficult to incorporate in a band-tail model, such as the existence of three emission peaks, the relative enhancement of blue emission for decreasing gap, the resonance features in the excitation spectra, and the polarization memory of photoluminescence.

In Sec. IV we showed that nonradiative recombination cannot be explained by multiphonon emission processes. We proposed that the nonradiative channel is strongly enhanced as a result of an increase of the density of distorted π-bonded configurations acting as acceptor sites, most of which are *not* ESR-active defects, in contrast with the assumptions of the band-tail model.[10] As the carbon skeleton densifies, it has been shown previously that an increase of local stress also

occurs simultaneously.[25] It is emphasized that geometrical distortions of the carbon matrix may have dramatic effects in the mixing of σ and π orbitals, leading to a decrease of both the optical gap[31] and the confinement of photogenerated excitonlike pairs. Stress-induced σ-π orbital mixing is expected to enhance the nonradiative tunneling mechanism. On the basis of Eq. (5), the increase of transition probability may result from both an increase of the acceptor site density and a decrease of the effective exciton reduced mass μ^* (i.e., an increase of radius a^*_{B1}) vs local density.

We observe resonant features in the PL excitation spectra corresponding to emission bands (a) and (b). They are attributed to some confinement of excitonlike species. Although structural studies do not give a proof of the existence of π-bonded nanoclusters in a-C:H films, some spatial confinement of photogenerated electron-hole pairs may take place in sp^2-rich regions of a-C:H films. We are not aware of any resonant features having been reported for the absorption coefficient spectra of a-C:H, which confirms that PL excitation spectroscopy is strongly site selective and provides a powerful local probe of molecularlike chromophores embedded in a solid matrix. The shape of the resonance features being dominated by heterogeneous broadening, our data suggest that the distribution of optical properties of light-emitting species is not too strongly broadened by disorder.

In contrast with previous hypothesis attributing the faster decay rate at higher $E_{\rm em}$ to the larger radiative rate of smaller units with more strongly confined carriers,[13] our model naturally explains this observation by the higher density of available electronic states in the upper part of the π^* state distribution (Fig. 7), leading to a smaller distance for electron tunneling.

Our hypothesis is consistent with the observed relative enhancement of the blue part of the emission spectrum as a function of decreasing optical gap, which may arise from the relatively larger change of the density of acceptor states close to the band edges. Similarly, our model predicts spectral modifications (such as red PL emission fatigue) for defect creation induced by intense laser illumination or by ion irradiation of a-C:H films, because defects localized near midgap (represented by hatched areas in Fig. 7) would induce a preferential quenching of the red part of the broad emission spectrum.

As a conclusion, the results of this investigation provide a substantial basis for understanding the recombination of confined electron-hole pairs. To describe PL properties of a-C:H we have proposed (Fig. 7) a local configuration coordinate diagram for light-emitting species and a band diagram for the matrix electronic properties. In this picture, the dependence of the PL decay rate on the emission energy $E_{\rm em}$ represents a mapping of the density of energy levels corresponding to distorted acceptor sites of the host matrix in the vicinity of a chromophore. Time-resolved studies of the PL intensity and PL anisotropy decays are currently being performed to understand the transfer mechanisms in amorphous carbon.

ACKNOWLEDGMENTS

We are grateful to M. N. Berberan-Santos for stimulating discussions, and to V. Chu who contributed to the steady-state PL measurements. This work was supported by a grant from the CNRS-ICCTI exchange program and by Project PRAXIS 3/3.1/MMA/1901/95.

[1] U. Rauscher, H. Bässler, D. D. C. Bradley, and M. Henneke, Phys. Rev. B **42**, 9830 (1990).
[2] H. Efstathiadis, Z. Akkerman, and F. W. Smith, J. Appl. Phys. **79**, 2954 (1996).
[3] J. Robertson, Philos. Mag. B **76**, 335 (1997).
[4] J. Angus and F. Jansen, J. Vac. Sci. Technol. A **6**, 1778 (1988).
[5] T. Heitz, B. Drévillon, C. Godet, and J. E. Bourée, Phys. Rev. B **58**, 13 957 (1998).
[6] M. Yoshimi, H. Shimizu, K. Hattori, H. Okamoto, and Y. Hamakawa, Optoelectronics **7**, 69 (1992).
[7] J. Robertson, in *Materials Issues in Vacuum Microelectronics*, edited by T. Felter, C. Holland, L. Pan, and W. Zhu, MRS Symposia Proceedings No. 509 (Materials Research Society, Pittsburgh, 1998).
[8] C. W. Chen and J. Robertson, J. Non-Cryst. Solids **227**, 602 (1998).
[9] S. V. Chernyshov, E. I. Terukov, V. Vassilyev, and A. S. Volkov, J. Non-Cryst. Solids **134**, 218 (1991).
[10] J. Robertson, Phys. Rev. B **53**, 16 302 (1996).
[11] Rusli, G. A. J. Amaratunga, and J. Robertson, Phys. Rev. B **53**, 16 306 (1996).
[12] F. Giorgis, F. Giuliani, C. F. Pirri, A. Tagliaferro, and E. Tresso, J. Non-Cryst. Solids **227**, 565 (1998).
[13] J. Cernogora, Phys. Status Solidi B **201**, 303 (1997).
[14] R. A. Street, Adv. Phys. **30**, 593 (1979).
[15] R. A. Street, *Hydrogenated Amorphous Silicon* (Cambridge University Press, Cambridge, 1991).
[16] C. Godet, in *Amorphous Carbon: State of the Art*, edited by S. R. P. Silva, J. Robertson, W. I. Milne, and G. A. J. Amaratunga (World Scientific, Singapore, 1998), p. 186.
[17] S. Schütte, S. Will, H. Mell, and W. Fuhs, Diamond Relat. Mater. **2**, 1360 (1993).
[18] S. Liedtke, K. Jahn, F. Finger, and W. Fuhs, J. Non-Cryst. Solids **97**, 1083 (1987).
[19] M. Koos, I. Pocsik, and L. Toth, J. Non-Cryst. Solids **164-166**, 1151 (1993).
[20] R. Etemadi, C. Godet, J. Perrin, B. Drévillon, J. Huc, J. Y. Parey, J. C. Rostaing, and F. Coeuret, J. Vac. Sci. Technol. A **15**, 320 (1997).
[21] C. Godet, T. Heitz, J. E. Bourée, B. Drévillon, and C. Clerc, J. Appl. Phys. **84**, 3919 (1998).
[22] F. Demichelis, C. F. Pirri, and A. Tagliaferro, Diamond Relat. Mater. **1**, 298 (1992).
[23] A. R. Forouhi and I. Bloomer, Phys. Rev. B **34**, 7018 (1986).
[24] M. D. Galanin, *Luminescence of Molecules and Crystals* (Cambridge International Science Publishing, Cambridge, 1996).
[25] T. Heitz, Ph.D. thesis, Ecole Polytechnique, France, 1998.
[26] J. E. Bourée, C. Godet, B. Drévillon, R. Etemadi, T. Heitz, J. Cernogora, and J. L. Fave, J. Non-Cryst. Solids **198-200**, 623 (1996). A typical spectrum is shown in Ref. 13 [Fig. 1(d)].

[27] S. Xu, M. Hundhausen, J. Ristein, B. Yan, and L. Ley, J. Non-Cryst. Solids **164-166**, 1127 (1993).
[28] J. E. Bourée, T. Heitz, C. Godet, B. Drévillon, J. P. Conde, V. Chu, M. N. Berberan-Santos, and A. Fedorov, J. Non-Cryst. Solids **227**, 574 (1998).
[29] T. Heitz, C. Godet, J. E. Bourée, B. Drévillon, V. Chu, J. P. Conde, and C. Clerc, in *Flat-Panel Display Materials*, edited by G. Parsons, T. S. Fahlen, S. Morozumi, C. Seager, and C. C. Tsai, MRS Symposia Proceedings No. 508 (Materials Research Society, Pittsburgh, 1998).
[30] R. W. Collins, Mater. Sci. Forum **52&53**, 341 (1989).
[31] J. Robertson, Diamond Relat. Mater. **4**, 297 (1995).
[32] S. Kivelson and C. D. Gelatt, Phys. Rev. B **26**, 4646 (1982).
[33] F. J. Clough, W. I. Milne, B. Kleinsorge, J. Robertson, G. A. J. Amaratunga, and B. N. Roy, Electron. Lett. **32**, 498 (1996).
[34] A. Tagliaferro (private communication).
[35] I. D. W. Samuel, B. Crystall, G. Rumbles, P. L. Burn, A. B. Holmes, and R. H. Friend, Chem. Phys. Lett. **213**, 472 (1993).
[36] W. Lormes, M. Hundhausen, and L. Ley, J. Non-Cryst. Solids **227**, 570 (1998).
[37] M. N. Berberan-Santos, A. Fedorov, T. Heitz, C. Godet, J. E. Bourée, and J. P. Conde, J. Non-Cryst. Solids (to be published).
[38] T. Frauenheim, P. Blaudeck, U. Stephan, and G. Jungnickel, Phys. Rev. B **48**, 4823 (1993).
[39] C. Godet, T. Heitz, J. E. Bourée, B. Bouchet, J. Dixmier, and B. Drévillon, Solid State Commun. **111**, 293 (1999).